


Article

Duplex Treatment of AISI 420 Steel by RF-ICP Nitriding and CrAlN Coating Deposition: The Role of Nitriding Duration

Dmitrii Vladimirovich Sidelev , Ekaterina Dmitrievna Voronina and Egor Borisovich Kashkarov 

School of Nuclear Science & Engineering, Tomsk Polytechnic University, 30 Lenina av., Tomsk 634050, Russia

* Correspondence: sidelevdv@tpu.ru; Tel.: +7-3822-70-17-77 (ext. 2518)

Abstract: The duplex treatment of AISI 420 steel samples by nitriding in a radiofrequency inductively coupled plasma (RF-ICP) discharge of Ar + N₂ + H₂ atmosphere followed by CrAlN coating deposition was performed in this study. The influence of plasma nitriding (PN) duration (10, 20, 40, and 60 min) on the structural and functional properties of the duplex-treated samples was determined. A non-linear dependence of AISI 420 steel nitriding kinetics was found on the square root of the PN duration. The thicknesses of the compound layer (CL) and nitrogen diffusion zone (DZ) in the samples and their phase composition resulted in different critical loads of coating failures under adhesion tests. Increasing the load-bearing capacity by the PN caused coating hardening in duplex-treated samples. The role of the PN duration on the wear characteristics of the AISI 420 steel samples after the duplex treatment has been discussed. Corrosion tests of AISI 420 steel demonstrated the significant enhancement (5–67 times) of its corrosion resistance in a 3.5 wt.% NaCl solution after duplex treatment.

Keywords: CrAlN coating; duplex treatment; coating deposition; plasma nitriding; radiofrequency inductively coupled plasma (RF-ICP)



Citation: Sidelev, D.V.; Voronina, E.D.; Kashkarov, E.B. Duplex Treatment of AISI 420 Steel by RF-ICP Nitriding and CrAlN Coating Deposition: The Role of Nitriding Duration. *Coatings* **2022**, *12*, 1709. <https://doi.org/10.3390/coatings12111709>

Academic Editor: Alessandro Patelli

Received: 21 September 2022

Accepted: 5 November 2022

Published: 9 November 2022

Publisher's Note: MDPI stays neutral with regard to jurisdictional claims in published maps and institutional affiliations.



Copyright: © 2022 by the authors. Licensee MDPI, Basel, Switzerland. This article is an open access article distributed under the terms and conditions of the Creative Commons Attribution (CC BY) license (<https://creativecommons.org/licenses/by/4.0/>).

1. Introduction

Stainless steels with a high chromium concentration (e.g., AISI 420, AISI 304, AISI 316, etc.) are widely used as base materials for producing different components and tools in the machinery, biomedical, chemical, and nuclear industries. This is due to their good corrosion resistance and low cost. Coating deposition is often used to modify surface properties (corrosion, wear and oxidation resistance, wettability, or other functional parameters) [1–3]. However, the critical issue of coating deposition is the adhesion strength of a coating to a substrate material. Poor coating adhesion can be caused by a strong difference in mechanical properties between the coating and substrate materials [4]. Coating adhesion can strongly influence the corrosion behavior of coated steel, especially under different factors, such as aggressive environment and mechanical loading. Several methods, such as substrate heating, ion bombardment or mixing, deposition of gradient coatings, and others [5–7], are often used to enhance coating adhesion. However, hard coatings, e.g., nitride-based coatings such as CrN, TiAlN, CrAlN, and TiAlSiN, are not the only factors involved [8]. To reduce the difference in mechanical properties between hard coatings and substrate material, substrate hardening by plasma nitriding (PN) is in high demand. The combination of PN and coating deposition can be used in one technological process, known as duplex treatment [9–14].

PN can be performed using various types of plasma source based on radiofrequency inductively coupled plasma (RF-ICP) [15–18], direct current (DC) glow [19,20] or arc discharges [21], microwave electron cyclotron (ECR) plasma [22], and others [23]. Unlike other techniques, PN based on RF-ICP has a higher nitriding rate [17]. The RF assistance to a DC plasma source was used to increase the nitriding kinetics of AISI H13 tool steel [18]. The

RF-ICP sources can create a highly reactive plasma at relatively low pressure, which corresponds to an operation range of the physical vapor deposition techniques used for coating deposition [16,17]. Indeed, the RF-ICP source can even operate as an atmospheric source for plasma immersion ion implantation performing at low nitriding temperature [24]. Another important point of applying the RF-ICP for PN is caused by the use of RF-ICP assistance in coating deposition, which has been suggested in some studies [25–27]. Therefore, in view of commercial tasks, a high nitriding rate and using a RF-ICP source during both PN and coating deposition can be beneficial in comparison with other PN techniques. However, the surface morphology and structure of the nitrided steels can be strongly changed under the RF-ICP nitriding as plasma species are directed to a substrate material due to biasing. The phase composition and surface roughness of the nitride steels can be modified by varying the amplitude of substrate biasing. Some studies have stated that an outer compound layer (CL) composed of brittle γ -Fe₄N and ϵ -Fe₂₋₃N phases on the surface of nitrided steels can decrease wear resistance [28]. Conversely, the presence of CL can be advantageous due to it improving the coating adhesion of duplex-treated samples, because CL will work as an interlayer between a hard outer coating and ductile nitrogen-expanded steels [29]. However, CL can be decomposed to CrN and α -Fe during coating deposition due to heating of the substrate and/or ion bombardment [30], leading to a higher difference in hardness between the coating and the substrate material. Therefore, mechanical pre-treatment (polishing) of nitrided steels is often applied before coating. The samples should be polished prior to the coating process because they should have some surface roughness parameters after the duplex treatment according to their industrial applications. Nevertheless, the importance of PN and coating deposition in one technological process is beneficial from an economical point of view. As contrary results on the influence of CL are presented in the literature, additional studies should be performed to reveal this dependence. Therefore, this article aims to analyze the influence of PN duration on the surface state of steel and its functional properties after CrAlN coating deposition. In this study, the CrAlN coating was deposited as a stage of the duplex treatment of AISI 420 steel because this coating has high hardness and wear characteristics, which are good protective properties for corrosion environments including O- and/or H-mediums [31–33].

2. Experimental Details

2.1. Duplex Treatment

Stainless steel (AISI 420) substrates were treated using duplex technology based on plasma nitriding in an RF-ICP discharge, along with deposition of a CrAlN coating using magnetron sputtering. The AISI 420 steel contains C (0.15 wt.%), Cr (12.5 wt.%), Mn (1 wt.%), Si (1 wt.%), P (0.03 wt.%), and Fe balance. The experimental scheme of the installation is shown in Figure 1. Initially, the substrates (\varnothing 25 mm and thickness of 4 mm) were ground and polished using SiC sandpapers with a grit of P400→P2500. The substrates were then cleaned in an ultrasonic bath with alcohol (98%) for 10 min and then dried with compressed air for 2 min. Initial AISI 420 steel samples did not undergo any preliminary treatment procedures before plasma nitriding or coating deposition. Their hardness was equal to ~2 GPa.

The plasma nitriding of the samples was performed using an RF-ICP source (RPG-128, Laboratory of Vacuum Technology Plus, LLC, Moscow, Russia) [34]. The RF-ICP source was mounted on the top wall of the vacuum chamber and connected to a COMDEL CX-1250 RF power supply (operation frequency—13.56 MHz). The following operation parameters were used in the nitriding process: substrate temperature—470 °C, operating pressure—0.8 Pa, substrate bias potential—(−80) V, and power of the RF-ICP source—1.25 kW. A gas mixture of Ar, N₂, and H₂ was injected into the vacuum chamber in the ratio of 4:2:1. The duration of the plasma nitriding process was equal to 10, 20, 40, and 60 min.

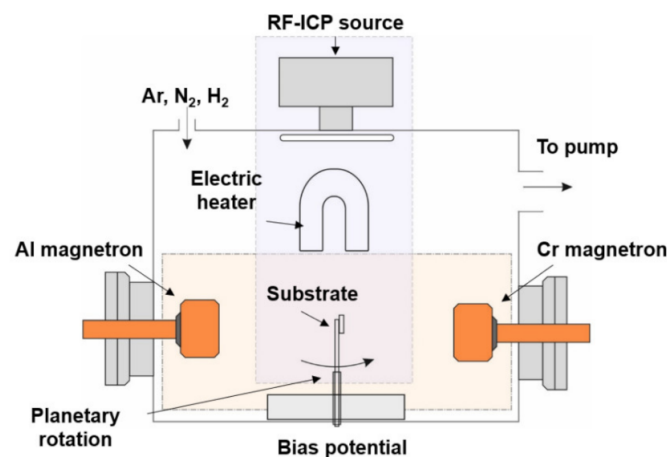


Figure 1. Scheme of the experimental installation for the duplex treatment.

The deposition of CrAlN coating was performed using two planar magnetrons equipped with a middle-frequency direct current power supply APEL-M-5PDC (Applied Electronics, Tomsk, Russia). The thickness of the coating was $\sim 1.7 \mu\text{m}$. The following operation parameters for the coating deposition were used: operating pressure—0.35 Pa, Ar flow rate—13.5 sccm, N_2 flow rate—13.5 sccm, deposition time—120 min, substrate bias potential—(−50) V, discharge power densities for Cr and Al targets—18.0 and 53.5 W/cm^2 , respectively. The substrates were planetary rotated during the coating deposition. The CrAlN coating was also deposited on the AISI 420 substrate without nitriding for comparison of their functional properties. In this article, for a simpler distinction of the samples, they will be hereinafter referred to as “WN” (without nitriding), “N10” (with 10 min nitriding), “N20” (with 20 min nitriding), “N40” (with 40 min nitriding), and “N60” (with 60 min nitriding).

2.2. Sample Characterization

The crystal structure of the samples was investigated by an X-ray diffractometer Shimadzu XRD 7000S with $\text{Cu-K}\alpha$ radiation (40 kV, 30 mA) from 10° to 90° with a scanning step of 0.0143° . The phase composition of the samples was analyzed using the ICDD-4+ database. Surface roughness was measured using a three-dimensional optical profilometer Micro Measure 3D Station (STIL, Aix-en-Provence, France). Five surface scans with a length of 3 mm were carried out to determine the arithmetic mean roughness, R_a , and the ten-point mean roughness, R_z , in all samples. An optical microscope (Axiovert 200MAT, Zeiss, Jena, Germany) and scanning electron microscope (SEM, Hitachi S-3400N, CSEM, Tokyo, Japan), equipped with an energy-dispersive X-ray spectroscopy (EDS) attachment, were used to investigate the cross-section microstructure of the samples. The SEM study was carried out using the equipment of the CSU NMNT TPU, supported by the RF MES project #075-15-2021-710.

The adhesion of the CrAlN coatings was measured using a Micro-Scratch Tester MST-S-AX-0000 (CSEM, Neuchâtel, Switzerland) with a Rockwell intender (radius of $100 \mu\text{m}$). The load range was equal to 0.1–30.0 N. The scratch length was 5 mm, and three scratch lines were made for each sample. After the tests, the adhesion lines were analyzed using an optical microscopy. The coating hardness was measured using an NHT² nanohardness tester (CSM Instruments, Peseux, Switzerland) with BT-59 indenter (Berkovich type). The load on the indenter was varied in the range of 10–250 mN. The measurements of the coating hardness were performed on the outer surface of the samples. The hardness of the nitrided layers was studied using a KB10 hardness tester with a Vickers indenter. The load on the indenter was 20 mN. The hardness measurements were performed on the cross-section of the samples from the coating/substrate interface up to $70 \mu\text{m}$. The wear resistance of the samples was studied using a TNT-S-AX0000 tribometer (CSEM, Switzerland). The scheme of a ball-on-disc with an Al_2O_3 counter-body was used. The

track radius was equal to 2.5 mm, and the rotation rate and the indenter load were 50 mm/s and 5 N, respectively. Sliding distances were equal to 237 and 98 m for samples after duplex treatment and coating deposition, respectively. After the wear tests, the specific wear coefficient of the samples was calculated by measuring the track profile using optical profilometry. The corrosion resistance of samples was determined by a potentiodynamic polarization method in a 3.5 wt.% NaCl solution using a potentiostat–galvanostat P-45X equipped with a three-electrode electrochemical cell. Potentiodynamic polarization tests were performed at room temperature ($\sim 25^\circ\text{C}$), and the working area of the samples was equal to 0.3 cm^2 . The reference electrode was a AgCl electrode (4.2 M KCl), while a counter electrode was made from high-purity graphite. Before taking measurements, each sample was kept in the solution at open circuit potential for at least 2000 s to compensate charges. Potentiodynamic polarization tests were then carried out in a potential range from -700 to 2000 mV , with a scan rate of 0.5 mV/s .

3. Results

3.1. Crystal Structure

Figure 2 shows the XRD patterns of the samples after the duplex treatment (N10, N20, N40, and N60) and the sample with CrAlN coating without nitriding (WN). The WN sample has reflections at angles of 32.4° , 37.1° , and 63.5° that correspond to CrN and AlN phases in the CrAlN coating. The main reflections of this sample are from the body-centered cubic (bcc) α -Fe phase of the initial substrate material (AISI 420 stainless steel).

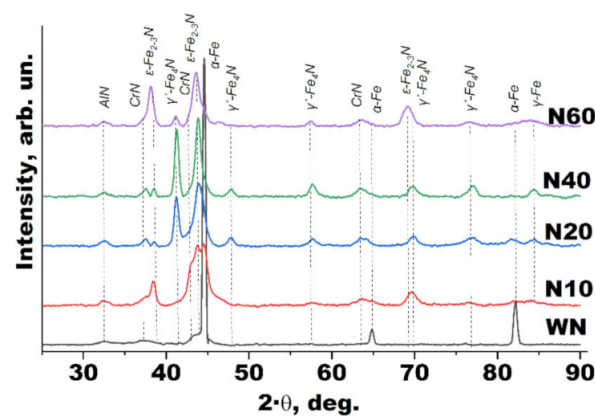


Figure 2. XRD patterns of AISI 420 samples after duplex treatment with the PN duration of 10 (N10), 20 (N20), 40 (N40), and 60 (N60) min. The WN sample is the AISI 420 substrate with CrAlN coating.

The samples after the duplex treatment also have CrN and AlN reflections related to the deposited coating, and the phases corresponded to the steel after the PN. There are additionally found solid solutions of austenitic Fe (γ -Fe phase) and iron nitrides, such as γ' -Fe₄N and ϵ -Fe_{2.3}N phases. The increase in the PN duration from 10 to 40 min leads to a rise in the γ' -Fe₄N intensities at 41.5° , 48.2° , and 76.9° . The XRD pattern of the N60 sample is noticeably changed from other samples. The intensities of Fe_{2.3}N phases at 38.3° and 69.1° significantly increased, while the intensity of the γ' -Fe₄N phase at 41.5° , 48.2° , and 76.9° decreased after 60 min nitriding.

3.2. Cross-Section Microstructure

Figure 3 shows optical images of the cross-section microstructure of the samples after the duplex treatment. The CrAlN coating can be clearly seen on the outer surface of the samples. Underneath the coating, the CL, including γ' -Fe₄N and ϵ -Fe_{2.3}N, is found, which is highlighted in Figure 3. The formation of the CL in the samples is confirmed by XRD data (Figure 2), which reveals the presence of the γ' -Fe₄N and ϵ -Fe_{2.3}N phases. The thickness of CL depends on the PN duration. The most pronounced CL is observed in the N40 sample. Beneath the CL, all samples have a nitrogen diffusion zone (DZ), and its thickness increased

from 5.1 to 25.9 μm as the PN duration changed from 10 to 40 min. The thickness of the DZ then decreased to $\sim 16.7 \mu\text{m}$ at 60 min PN.

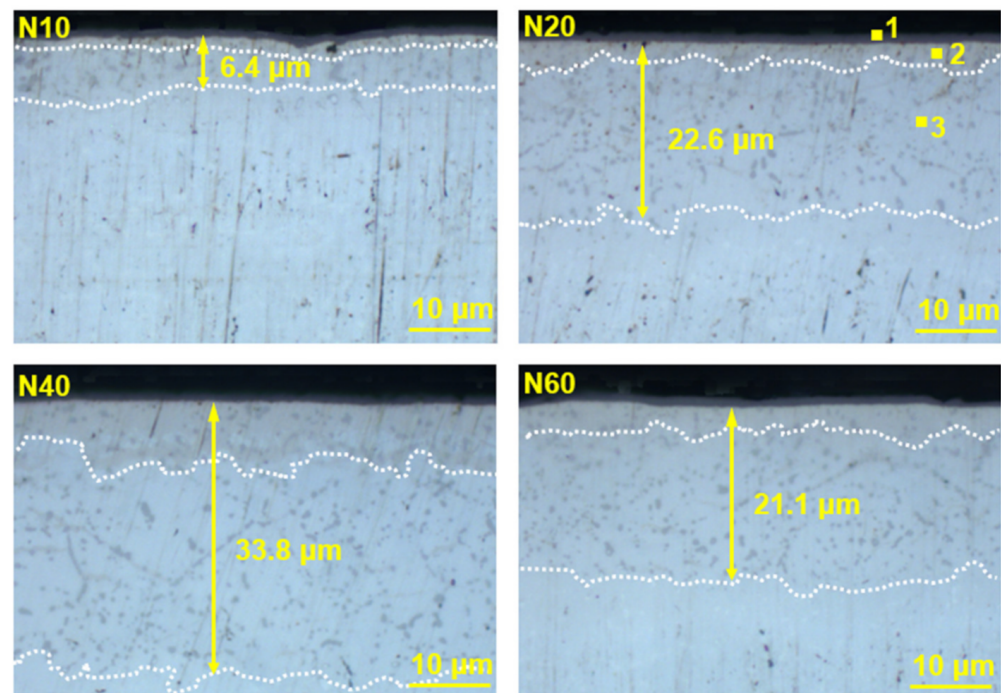


Figure 3. Optical images of the cross-section microstructure of the samples after the duplex treatment: 1—CrAlN coating; 2—compound layer (CL); 3—nitrogen diffusion zone (DZ). The averaged total thickness of the CL and DZ is added together.

Figure 4 presents the SEM image of the cross-section microstructure of the N40 sample. The EDS measurements revealed the elemental composition of the layers in the cross-section of the N40 sample. The CrAlN coating consisted of 25.5 at.% Al, 12.3 at.% Cr, and 53.9 at.% N. The presence of the Fe signal in the coating layer is due to a low thickness of the coating (1.7 μm), which leads to electron beam incidence on the steel substrate. The CL is composed of 16.8 at.% N, 9.5 at.% Cr, and 72.6 at.% Fe, which is in a good agreement with the published literature [35]. Underneath the CL, the DZ has 10.0 at.% N, 10.7 at.% Cr, and 78.8 at.% Fe. Moreover, some dark areas are observed in both the CL and the DZ (point 3) that corresponds to CrN precipitates. According to EDS, a non-treated steel with a small content of dissolved N (1.2 at.%) is observed underneath the DZ.

3.3. Surface Morphology

Figure 5 shows images of the surface morphology of the duplex-treated samples obtained by optical profilometry.

Figure 5e corresponds to the surface morphology of the WN sample. It can be seen that the surface of the coated steel is flat and uniform. Some continuous lines of peaks on surface can be formed under preliminary polishing of samples prior to coating. Samples after the duplex treatment (Figure 5a–d) had more non-uniform surface morphology, with peaks distributed on their surface. The change of surface morphology was caused by surface sputtering during the PN stage. As the PN duration increased from 10 to 60 min, the peaks on the surface had an increased height and diameter. Using surface morphology images, R_a and R_z parameters were calculated for the samples after duplex treatment. Figure 6 shows the dependence between the PN duration and the surface morphology (R_a and R_z) parameters of the samples. As the R_a and R_z parameters were determined after the duplex treatment of the samples, so the surface morphology was somewhat smoothed due to CrAlN coating deposition on the nitrated steel samples.

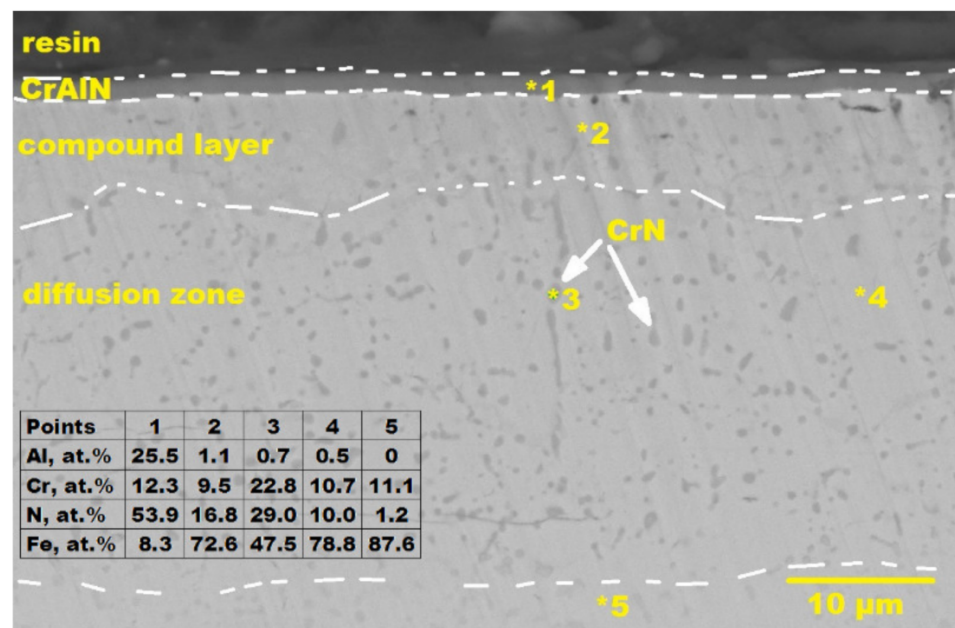


Figure 4. SEM image of the cross-section microstructure of the N40 sample and corresponding EDS data (in at.%).

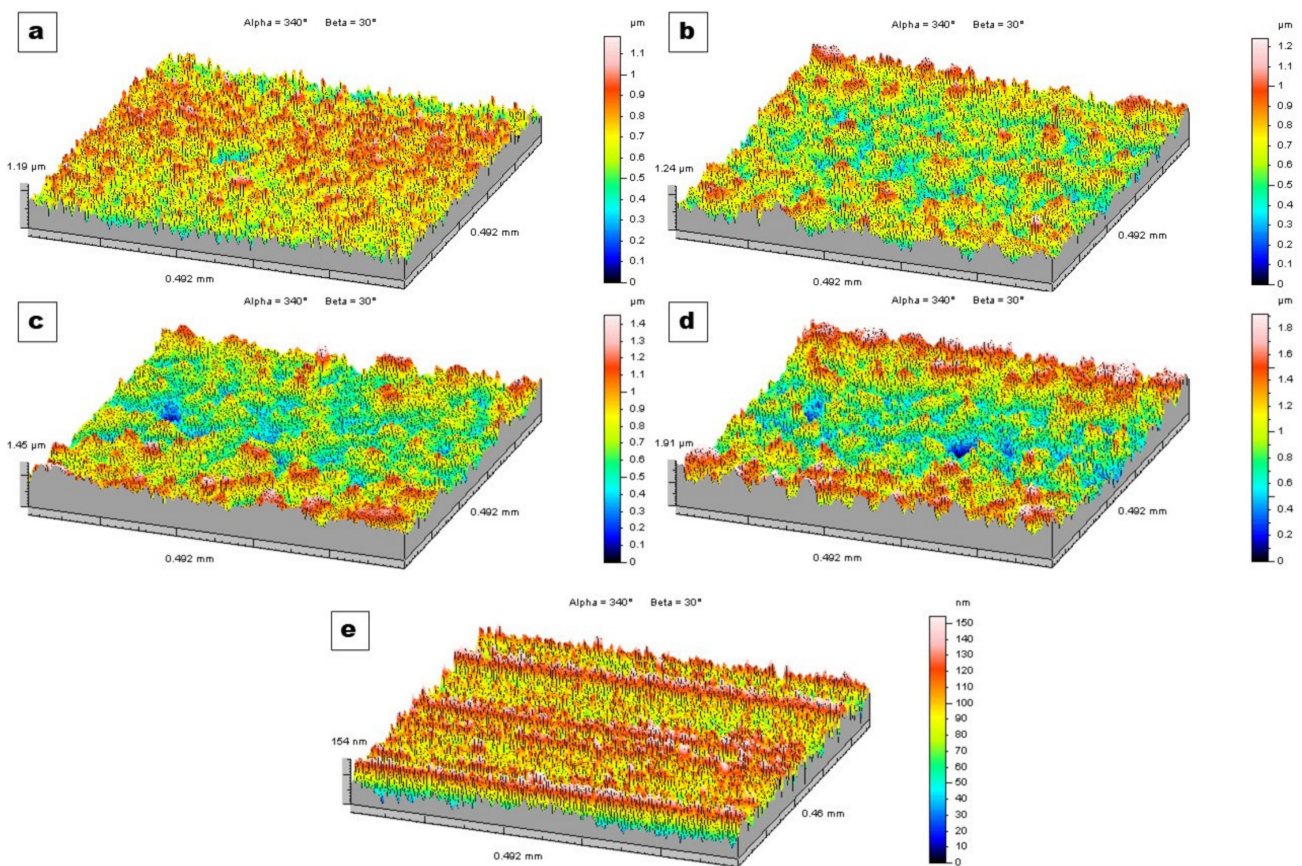


Figure 5. Images of surface morphology of duplex-treated samples depending on PN duration: (a)—N10, (b)—N20, (c)—N40, (d)—N60, and (e)—WN (with CrAlN coating and without PN).

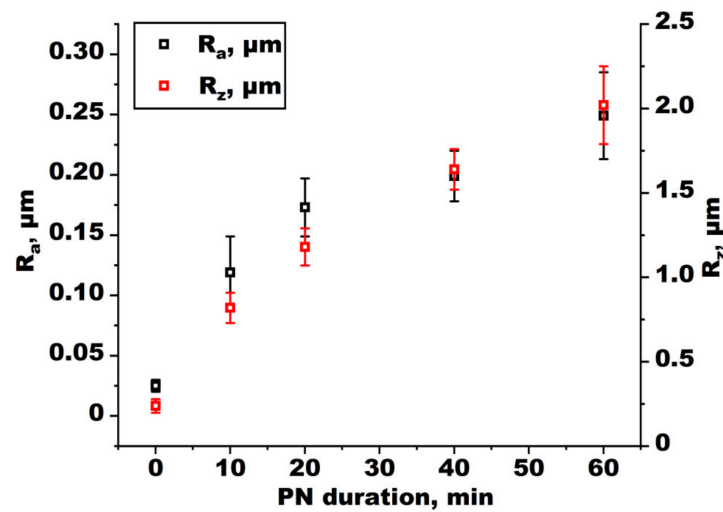


Figure 6. The dependence of R_a and R_z parameters on the PN duration.

The WN sample had the lowest R_a (0.03 μm) and R_z (0.24 μm) as this sample was only coated by CrAlN without PN processing. When the PN was applied during the shortest duration (10 min), parameters R_a and R_z both noticeably increased up to 0.12 and 0.82 μm , respectively. As the PN duration changed from 10 to 60 min, the increase in R_a and R_z of the nitrided samples was also observed up to 0.25 and 2.02 μm , respectively.

3.4. Hardness Measurements

In order to determine the hardness of the samples after the duplex treatment, two types of hardness measurements were performed. The coating hardness was measured using the nanoindentation technique on the sample surface by varying indentation loads in the range of 20–250 mN. The hardness distribution depending on the penetration depth is shown in Figure 7. The hardness of the initial AISI 420 steel is added for comparison. It can be seen that the penetration depth for the nitrided samples varies from 0.1 to 0.9 μm , which is approximately 6%–53% of the coating thickness (1.7 μm).

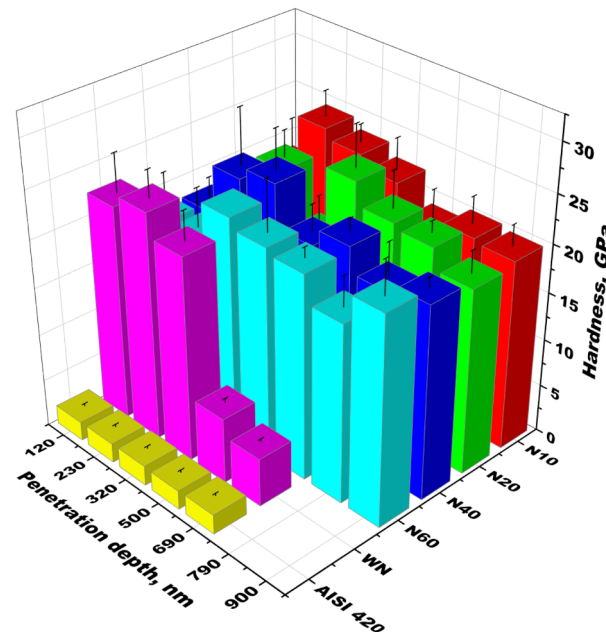


Figure 7. The dependences of the hardness of the samples on the penetration depth.

Taking into account the measurement errors, no visible dependence of the PN duration on the hardness was found. The hardness of the samples after the duplex treatment is the same over the range of penetration depths. The averaged hardness is equal to ~23 GPa. The WN sample has another hardness distribution over the penetration depth. The hardness is significantly reduced from 23 to 5–6 GPa, which corresponds to the hardness of the non-treated steel substrate.

The second type of hardness measurements include indentations with a constant indenter load over the cross-sections of the samples from the coating interface to the sample depth (Figure 8). Unfortunately, it is not possible to measure the hardness of the N10 sample due to the low thicknesses of the CL and DZ (Table 1).

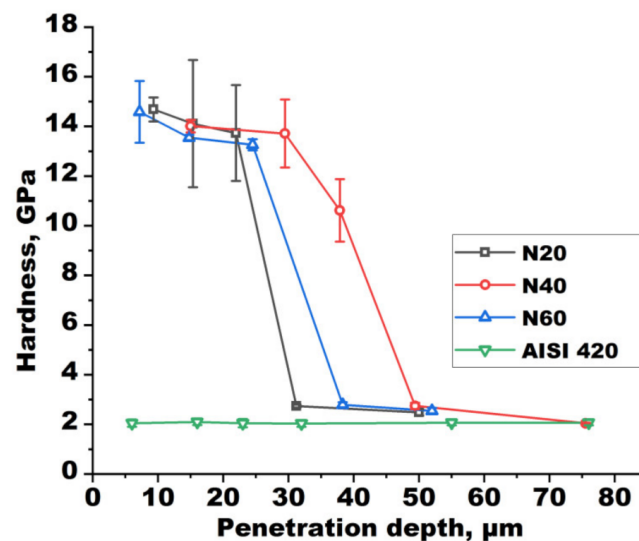


Figure 8. The hardness distributions of the cross-sections of the samples over a sample depth.

Table 1. The thickness of the CL and DZ layers and wear characteristics of the samples.

Sample	h_{CL} , μm	h_{DZ} , μm	W , $10^{-6} \cdot \text{mm}^3/(\text{m} \cdot \text{N})$	h_m , μm	h_s , μm
WN	-	-	1580	78.5 ± 2.3	76.8 ± 2.3
N10	1.3 ± 0.3	5.1 ± 1.0	7	3.1 ± 0.4	1.4 ± 0.4
N20	3.0 ± 0.9	19.6 ± 1.4	13	5.3 ± 0.2	3.6 ± 0.2
N40	7.9 ± 1.7	25.9 ± 1.3	4	2.3 ± 0.1	0.6 ± 0.1
N60	5.4 ± 1.1	16.7 ± 1.4	8	3.8 ± 0.3	2.1 ± 0.3

Note: h_{CL} —thickness of the CL; h_{DZ} —thickness of the DZ; h_m —maximal depth of the wear tracks; h_s —maximal depth of the wear tracks in steel substrate.

According to Figure 8, the hardness of the samples after the duplex treatment is significantly increased (~14 GPa) compared to the hardness of the initial (non-treated) AISI 420 steel (~2 GPa). Such high hardness of the duplex-treated samples is attributed to the formation of the CL at the coating/steel interface and the DZ in the depth of the samples. The observed hardness of the nitride steel samples is in a good agreement with the published data [16,17]. It can be clearly seen that a high hardness is observed throughout the whole depth of the CL and DZ; the hardness then decreases to 2–4 GPa, which are typical values for the non-treated steel.

3.5. Coating Adhesion

According to the acoustic curves obtained during the scratch testing of the samples and the optical images of the scratch tracks, the critical loads of first crack formation, coating chipping, and spallation were determined (Figure 9). The critical loads were averaged from the three scratch lines of each sample.

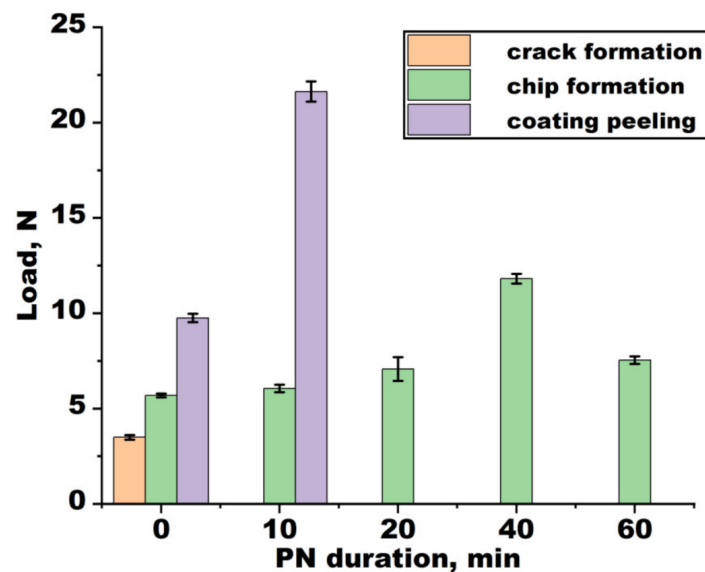


Figure 9. The critical loads of first crack formation, coating chipping, and spallation depending on the PN duration.

Three types of CrAlN coating failure were observed for the WN sample at the critical loads of 3.5, 5.7, and 9.8 N, respectively, when coating cracking, chipping, and delamination occurred. The samples after the duplex treatment have another scratching behavior. The N10 sample has only two types of coating failure (6.1 and 21.6 N), excluding cracking. Coating chipping only occurred on the samples after duplex treatment for 20–60 min. No other failures of the CrAlN coatings for these samples were observed up to 30 N. The increase in the PN duration from 10 to 40 min results in a 2-fold rise in the critical load of coating chipping (~11.8 N). For the N60 sample, coating chipping was observed at a lower indenter load of ~7.6 N.

3.6. Wear Resistance

The 3D profiles of wear tracks of the samples were obtained using optical profilometry; the specific wear coefficient (W) was then calculated using the followed formula:

$$W = \frac{V_w}{F \cdot l}, \quad (1)$$

where V_w —volume of wear track, mm^3 ; F —normal load, N; l —friction distance, m.

The dependence of the specific wear rate of the samples after the duplex treatment was plotted based on the PN duration (Figure 10), and the specific wear coefficient of the AISI 420 steel with CrAlN coating is added.

According to Figure 10, the PN can strongly improve the wear resistance of the AISI 420 steel samples, because the specific wear coefficient after the duplex treatment decreased in the range of two orders, unlike the WN sample. The WN sample had the specific wear coefficient of $\sim 1.6 \times 10^{-3} \text{ mm}^3/(\text{m} \cdot \text{N})$, while the duplex-treated samples were in the range of 4×10^{-6} – $1.3 \times 10^{-5} \text{ mm}^3/(\text{m} \cdot \text{N})$. The dependence of specific wear coefficients on the PN duration is non-linear. To identify this behavior, the maximum depth of the wear tracks (h_m) was calculated and summarized in Table 1. Based on the optical images and EDS data of the samples, the thicknesses of the layers were also calculated and added to Table 1. Taking into account the thickness of the CrAlN coating ($h_c = 1.7 \text{ }\mu\text{m}$), the maximal depth of the wear tracks in the steel substrate (h_s) can also be determined:

$$h_s = h_m - h_c. \quad (2)$$

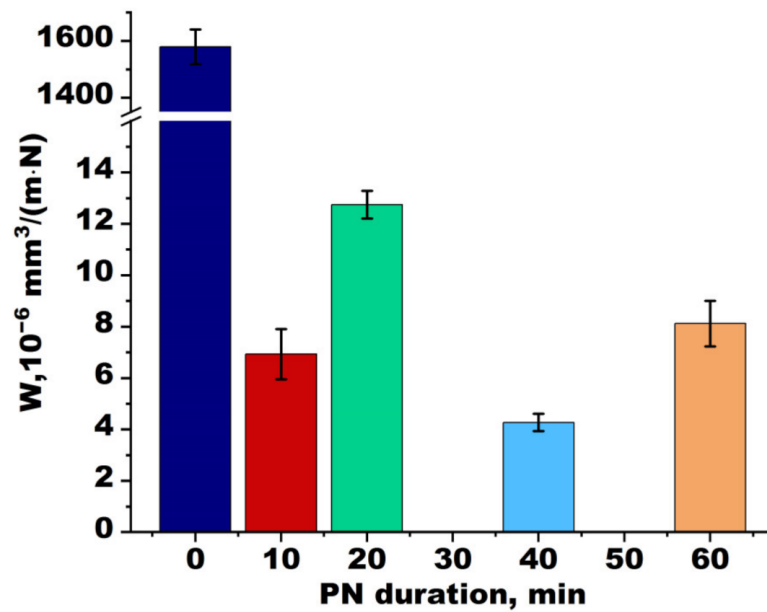


Figure 10. The dependence of specific wear coefficients of the samples based on the PN duration.

3.7. Corrosion Resistance

Figure 11 shows the potentiodynamic curves of the initial AISI 420 steel, steel with CrAlN coating, and steel after the duplex treatment. Parameters such as E_{corr} and j_{corr} were determined from the curves. The polarization resistance (R_p) was calculated based on the slope of the Tafel anodic (β_a) and cathodic (β_c) curves using the Stern–Geary equation [36]:

$$R_p = \frac{|\beta_a \cdot \beta_c|}{2.303 j_{corr} (\beta_a + \beta_c)} \tag{3}$$

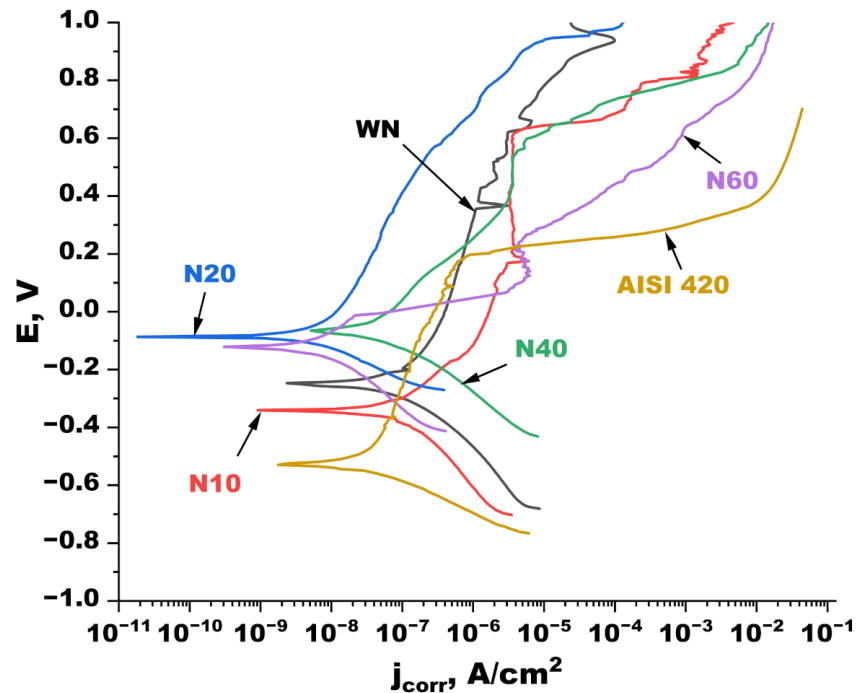


Figure 11. Potentiodynamic curves of initial AISI 420 steel substrates, with CrAlN coating (WN) and after the duplex treatment, depending on PN duration: N10 (10 min), N20 (20 min), N40 (40 min), and N60 (60 min).

Corrosion rate (CR) was obtained by the standard ASTM G 102-89 [37]. All corrosion parameters are summarized in Table 2.

Table 2. Corrosion parameters of samples.

Sample	j_{corr} , 10^{-9} A/cm ²	E_{corr} , mV	β_a , mV	β_c , mV	R_p , M Ω ·cm ²	CR, 10^{-4} mm/year
AISI 420	302.9	−334.5	−83	159	0.002	20
WN	15.7	−246.8	−57	60	0.32	1.2
N10	54.5	−340.4	−144	159	0.12	4.2
N20	5.1	−86.5	−113	233	0.19	0.4
N40	11.4	−65.1	−97	152	0.05	0.9
N60	4.0	−121.1	−110	133	0.70	0.3

Although AISI 420 steel demonstrates good corrosion resistance, the corrosion current density of the initial AISI 420 steel (3.1×10^{-7} A/cm²) was higher than that of the steel sample with CrAlN coating (1.6×10^{-8} A/cm²). Coatings with Al can usually improve the corrosion resistance of the substrate material due to the formation of Al₂O₃ protective scale in an aggressive environment [38]. Despite the change of mechanical properties of AISI 420 steel by the duplex treatment, it can also result in modifying its corrosion resistance. The N10 sample had higher j_{corr} (5.5×10^{-8} A/cm²) compared to the other duplex-treated samples ($(4.0\text{--}11.4) \times 10^{-8}$ A/cm²). Calculations of CR demonstrated the role of CrAlN coating deposition and duplex treatment on the corrosion of AISI 420 steel. It was found that the initial steel had 2.0×10^{-3} mm/year, while samples with CrAlN coating and after the duplex treatment had lower CR in a range of 3.0×10^{-5} to 4.2×10^{-4} mm/year.

4. Discussion

The duplex treatment of AISI 420 stainless steel using the RF-ICP source for plasma nitriding has higher nitriding rates in comparison with other nitriding methods [39–41]. A nitrided layer (CL + DZ) with a total thickness of 33.1 μm can be obtained for 40 min at a relatively low nitriding temperature of 470 °C (Figure 12). However, the thickness of the nitrided layers has a linear dependence on the square root of the PN duration only up to 40 min. This indicates the parabolic kinetics of the nitrided layer growth caused by a diffusion controlled process. A higher PN duration (60 min) revealed other nitriding kinetics. Indeed, as the phase composition of the outer layer of the nitrided steel changed during the PN stage, the nitriding rate can be noticeably decreased. According to the XRD data and optical images of the cross-section microstructures (Figures 2 and 3), a decrease in the total thickness of the CL and DZ is found when the intensities of the ϵ -Fe_{2.3}N reflections increased (40 → 60 min nitriding). The diffusion coefficients of nitrogen should not be assumed as a constant value in different phases. From the literature [42], it is equal to 5×10^{-8} and 9×10^{-10} – 4×10^{-9} mm²/s in γ' -Fe₄N and ϵ -Fe_{2.3}N at 470 °C, respectively. However, the PN using the RF-ICP source is also characterized by a surface sputtering as the bias potential (−80 V) was applied to the samples. A sputtering rate of γ' -Fe₄N and ϵ -Fe_{2.3}N was calculated using the following formula:

$$v = \frac{K \cdot j \cdot M_2}{N_A \cdot \rho \cdot q_e} \quad (4)$$

where K —sputtering yield, j —ion current density to a substrate (A/ μm^2), M_2 —molar weight of substrate material (g/mol), N_A —Avogadro's number (mol^{−1}), ρ —density of substrate material (g/ μm^3), q_e —elemental charge (C). Only argon ions were involved in the calculations of sputtering rates. The SRIM code [43] was used to determine sputtering yields. It was equal to 0.332 and 0.317 for the Fe₄N and Fe_{2.3}N layers, respectively. Thus, the sputtering rates of the Fe₄N and Fe_{2.3}N layers can be 140 and 105 $\mu\text{m}/\text{h}$, respectively. Based on the above calculations, the change of the phase composition of the surface layer during PN can result in a decrease in diffusion rate of 3.5, while sputtering rate can only drop by

1.3. Under these conditions, the nitrogen diffusion rate can be slowed down as a CL layer composed of ϵ -Fe₂₋₃N was formed, and the thickness of the nitrided layer can be decreased due to the surface sputtering.

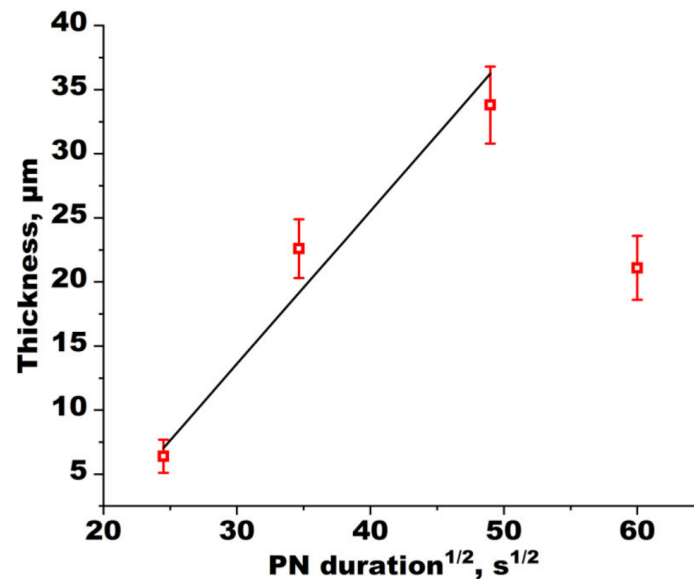


Figure 12. Thickness of the nitrided layer of AISI 420 steel samples as a function of the PN duration.

Sputtering of the AISI 420 steel samples during the PN stage also caused the changing R_a and R_z parameters of the samples after the duplex treatment, but it can become smoothed due to the followed deposition of the CrAlN coating by magnetron sputtering. However, significant changes in the surface morphology parameters of the samples occurred even after the short-term PN (10 min) stage and cannot be mitigated only by the coating deposition. It is more important that the PN results in a strong hardening of the surface region of the AISI 420 steel after the duplex treatment. Based on the hardness distributions (Figures 7 and 8), an increase in the surface hardness of the coating region up to 53% of the initial thickness of the coating is found, whereas the surface hardness is sharply reduced on the non-treated AISI 420 steel sample. Such an effect can be explained by increasing the load-bearing capacity of the nitrided steel substrates, because their hardness was increased by ~ 7 times compared to non-treated steel. This also works for the samples with a low thicknesses of CL (1.3 μm) and DZ (5.3 μm) after 10 min nitriding using the RF-ICP source. It is well known that the duplex treatment can lead to increased coating adhesion on the hardening substrate due to the enhanced load-bearing capacity of the nitrided substrate [8,12,14]. The same dependence was found in the present study. The increasing critical loads of coating chipping and the limitation of coating cracking under the scratch tests are observed in Figure 9. However, the formation of the thin CL and DZ in the nitrided steel cannot exclude a coating spallation at the experimental range of indentation loads (up to 30 N). Thicker nitriding of the steel substrate should be performed to improve coating adhesion. Moreover, the increased surface roughness ($R_a \sim 0.03 \rightarrow 0.21 \mu\text{m}$) can also result in better coating adhesion parameters because of a penetration of coating atoms in the surface grooves and pores of the nitrided steel, leading to enhanced bonding of the coating in comparison with deposition onto a polished surface [12,44]. Nevertheless, as the CL composed of the ϵ -Fe₂₋₃N phase forms on the outer surface, the coating adhesion will be decreased. Indeed, such CL has a brittle behavior compared to the nitrided layers consisting of the γ' -Fe₄N phase or DZ, which causes chipping of the coating during scratch testing. It is well observed when comparing the critical loads of the N40 and N60 samples (Figure 9).

The calculations of the wear characteristics of the samples indicated the role of PN duration in the duplex treatment of AISI 420 steel coated by CrAlN. According to Table 1,

the non-linear dependence of the specific wear characteristic is found based on the PN duration. Of course, the sample without the PN had the highest W , and the height of the wear tracks was significantly higher than that of the other samples due to the low hardness of the initial AISI 420 steel (~2 GPa). Any hardening resulted in better wear resistance to a minimum of two-orders of magnitude; however, this can be changed by varying the PN duration. Several factors can influence the wear characteristics of the duplex-treated samples.

Despite low adhesion parameters, the sample after 10 min PN had the highest wear resistance (Figure 10). As this sample had the thinnest CL layer (~1.3 μm), the surface region was mainly composed of the DZ (~5.1 μm). Indeed, the wear test of the N10 sample ended at the maximum depth corresponding to the interface between the CL and the DZ. The latter is usually characterized by good wear resistance [3,29]. The duplex-treated N20 sample had a specific wear coefficient that was twice as high as that of the previous one. The maximum height of the wear tracks in the steel substrate (~3.6 μm) was higher than that of the CL thickness (~3.0 μm). This indicates a failure of the CrAlN coating and the CL during the wear test leading to the enhanced wear rate. The strong increase in coating adhesion of the sample with the highest thicknesses of the DZ and the CL, which was mainly composed of the γ' -Fe₄N phase, and better load-bearing capacity of the nitrided substrate revealed the highest wear resistance of the N40 sample among all experimental samples. Indeed, this sample had the lowest depth of the wear tracks in the steel substrate (~2.3 μm), which corresponded to the contact of the counter-body ball with the CL and some wear of this layer up to a depth of ~0.6 μm when the wear test was finished. The next increase in W was caused by both an increase in the content of the brittle ϵ -Fe_{2,3}N phase in the CL and a decrease in the coating adhesion to the nitrided steel substrate.

The corrosion tests revealed a positive effect of surface treatment on the corrosion resistance of AISI 420 steel substrates. A strong decrease in corrosion rate was found after both the CrAlN coating deposition and the duplex treatment. Due to the presence of Al in the deposited coating, newly formed Al₂O₃ layers can enhance corrosion resistance, acting as a passive barrier on the sample surface [38]. However, PN processing can also influence the corrosion resistance of AISI 420 steel substrates. It is well known that the formation of the diffusion zone in stainless steel leads to a decrease in corrosion current density [39,45]. Therefore, better corrosion resistance should be observed for the N10 sample compared to that of the WN sample. However, the significant increase in R_p from 0.03 to 0.12 μm due to surface sputtering during the PN stage can deteriorate the corrosion current density. The samples after the duplex treatment with a longer PN stage (20, 40, and 60 min) had better corrosion resistance than the previous one. This is mainly due to the increase in thickness of the DZ and the formation of F_{2,3}N [39,46], which improved overall corrosion resistance. Therefore, the corrosion rate of AISI 420 steel can be decreased 17 times by CrAlN coating deposition and 5–67 times using the duplex treatment.

Taking into account both results of mechanical and corrosion tests, the duplex treatment of AISI 420 steel by plasma nitriding in RF-ICP discharge and CrAlN coating deposition can be an effective approach to modify the surface properties of AISI 420 steel.

5. Conclusions

AISI 420 steel samples were treated by a two-step process of plasma nitriding in Ar + N₂ + H₂ atmosphere using a radiofrequency inductively coupled plasma (RF-ICP) source and the deposition of a CrAlN coating by magnetron sputtering. The duration of plasma nitriding was varied from 10 to 60 min. The non-linear dependence of the nitriding rate of AISI 420 steel samples on the square root of the nitriding duration was found, which was caused by the high content of the ϵ -Fe_{2,3}N phase in the outer compound layer that limited the nitrogen diffusion rate. Higher nitriding duration resulted in a better load-bearing capacity of the nitrided substrate for magnetron-sputtered CrAlN coating under scratch testing. A strong increase in the critical loads of coating failures was found with increasing ϵ -Fe_{2,3}N content in the compound layer. The wear resistance of the duplex-treated AISI

420 steel samples depended on the thickness of the compound layer and nitrogen diffusion zone as well as the presence of the ϵ -Fe₂3N phase in the surface region of the nitrided steel. Corrosion tests of AISI 420 steel samples revealed a strong increase (67 times) in corrosion resistance in a 3.5 wt.% NaCl solution after its duplex treatment.

Author Contributions: Conceptualization, D.V.S.; methodology, D.V.S.; validation, D.V.S. and E.D.V.; formal analysis, D.V.S. and E.D.V.; investigation, D.V.S. and E.D.V.; resources, D.V.S. and E.B.K.; data curation, E.D.V.; writing—original draft preparation, E.D.V.; writing—review and editing, D.V.S.; visualization, E.D.V.; supervision, D.V.S.; project administration, D.V.S.; funding acquisition, E.B.K. All authors have read and agreed to the published version of the manuscript.

Funding: The research was funded by Governmental Program (Project No. FSWW-2021-0017).

Institutional Review Board Statement: Not applicable.

Informed Consent Statement: Not applicable.

Data Availability Statement: Not applicable.

Acknowledgments: This research was supported by the TPU development program.

Conflicts of Interest: The authors declare no conflict of interest.

References

1. Vereschaka, A.; Milovich, F.; Andreev, N.; Sitnikov, N.; Alexandrov, I.; Muranov, A.; Mikhailov, M.; Tatarkanov, A. Efficiency of application of (Mo, Al) N-based coatings with inclusion of Ti, Zr or Cr during the turning of steel of nickel-based alloy. *Coatings* **2021**, *11*, 1271. [[CrossRef](#)]
2. Vereschaka, A.; Seleznev, A.; Gaponov, V. Wear resistance, patterns of wear and plastic properties of Cr,Mo-(Cr,Mo,)N-(Cr,Mo,Al)N composite coating with a nanolayer structure. *Coatings* **2022**, *12*, 758. [[CrossRef](#)]
3. Kiryukhantsev-Korneev, P.V.; Sytchenko, A.D.; Vorotilo, S.A.; Klechkovskaya, V.V.; Lopatin, V.Y.; Levashov, E.A. Structure, oxidation resistance, mechanical, and tribological properties of N- and C-Doped Ta-Zr-Si-B hard protective coatings obtained by reactive D.C. magnetron sputtering of TaZrSiB ceramic cathode. *Coatings* **2020**, *10*, 946. [[CrossRef](#)]
4. Claver, A.; Randulfe, J.J.; Palacio, J.F.; Fernández de Ara, J.; Almandoz, E.; Montalá, F.; Colominas, C.; Cot, V.; García, J.A. Improved adhesion and tribological properties of AlTiN-TiSiN coatings deposited by DCMS and HiPIMS on nitrided tool steels. *Coatings* **2020**, *11*, 1175. [[CrossRef](#)]
5. Ward, L.; Junge, F.; Lampka, A.; Dobbertin, M.; Mewes, C.; Wienecke, M. The effect of bias voltage and gas pressure on the structure, adhesion and wear behavior of diamond like carbon (DLC) coatings with Si interlayers. *Coatings* **2014**, *4*, 214–230. [[CrossRef](#)]
6. Rabadzhyska, S.; Kotlarski, G.; Shipochka, M.; Rafailov, P.; Ormanova, M.; Strijkova, V.; Dimcheva, N.; Valkov, S. Duplex surface modification of 304-L SS substrates by an electron-beam treatment and subsequent deposition of diamond-like carbon coatings. *Coatings* **2022**, *12*, 401. [[CrossRef](#)]
7. Hu, J.; Wang, J.; Jiang, J.; Yang, X.; Xu, H.; Li, H.; Guo, N. Effect of heating treatment on the microstructure and properties of Cr–Mo duplex-alloyed coating prepared by double glow plasma surface alloying. *Coatings* **2019**, *9*, 336. [[CrossRef](#)]
8. Podgornik, B.; Sedlaček, M.; Žužek, B.; Guštin, A. Properties of tool steels and their importance when used in a coated system. *Coatings* **2020**, *10*, 265. [[CrossRef](#)]
9. Naeem, M.; Awan, S.; Shafiq, M.; Raza, H.; Iqbal, J.; Díaz-Guillén, J.C.; Sousa, R.R.M.; Jelani, M.; Abrar, M. Wear and corrosion studies of duplex surface-treated AISI-304 steel by a combination of cathodic cage plasma nitriding and PVD-TiN coating. *Ceram. Int.* **2022**, *48*, 21514–21523. [[CrossRef](#)]
10. Yumusak, G.; Leyland, A.; Matthews, A. A microabrasion wear study of nitrided α -Ti and β -TiNb PVD metallic thin films, pre-deposited onto titanium alloy substrates. *Surf. Coat. Technol.* **2022**, *442*, 128423. [[CrossRef](#)]
11. Uzun, Y. Tribocorrosion properties of plasma nitrided, Ti-DLC coated and duplex surface treated AISI 316L stainless steel. *Surf. Coat. Technol.* **2022**, *441*, 128587. [[CrossRef](#)]
12. Weinhold, T.; Dalke, A.; Schramm, A.; Biermann, H. Sliding wear behavior of duplex coatings with different plasma nitride layers and a Cr-Al-Ti-B-N coating. *Eng. Rep.* **2022**, *4*, 12377. [[CrossRef](#)]
13. Dalke, A.; Weinhold, T.; Schramm, A.; Wüstefeld, C.; Ratayski, U.; Sochora, V.; Biermann, H.; Rafaja, D. Microstructure and adhesion characteristics of duplex coatings with different plasma-nitrided layers and a Cr-Al-Ti-B-N physical vapor deposition coating. *Eng. Rep.* **2020**, *4*, 12364. [[CrossRef](#)]
14. Grenadyorov, A.S.; Solovyev, A.A.; Oskomov, K.V. The effect of duplex processing on the mechanical properties of grade 316L stainless steel. *Tech. Phys. Lett.* **2020**, *46*, 1060–1063. [[CrossRef](#)]
15. Meshcheryakova, E.A.; Kaziev, A.V.; Zibrov, M.S.; Stepanova, T.V.; Berdnikova, M.M.; Kharkov, M.M.; Pisarev, A.A. Investigation of parameters of inductively coupled plasma and its use in steel nitriding. *Bull. Russ. Acad. Sci. Phys.* **2016**, *80*, 175–179. [[CrossRef](#)]

16. El-Hossary, F.M.; Negm, N.Z.; Abd El-Rahman, A.M.; Hammad, M.; Templier, C. Duplex treatment of AISI 304 austenitic stainless steel using rf nitriding and dc reactive magnetron sputtering of titanium. *Surf. Coat. Technol.* **2008**, *202*, 1392–1400. [[CrossRef](#)]
17. Valencia-Alvarado, R.; de la Piedad-Beneitez, A.; de la Rosa-Vázquez, J.; López-Callejas, R.; Barocio, S.R.; Godoy-Cabrera, O.G.; Mercado-Cabrera, A.; Peña-Eguiluz, R.; Muñoz-Cas, A.E. Nitriding of AISI 304 stainless steel in a 85% H₂/15% N₂ mixture with an inductively coupled plasma source. *Vacuum* **2008**, *82*, 1360–1363. [[CrossRef](#)]
18. Paosawatyanong, B.; Pongsopa, J.; Visuttipitukul, P.; Bhanthumnavin, W. Nitriding of tool steel using dual DC/RFICP plasma process. *Surf. Coat. Technol.* **2016**, *306*, 351–357. [[CrossRef](#)]
19. Borgioli, F.; Fossati, A.; Matassini, G.; Galvanetto, E.; Bacci, T. Low temperature glow-discharge nitriding of a low nickel austenitic stainless steel. *Surf. Coat. Technol.* **2010**, *204*, 3410–3417. [[CrossRef](#)]
20. Borgioli, F.; Fossati, A.; Galvanetto, E.; Bacci, T. Glow-discharge nitriding of AISI 316L austenitic stainless steel: Influence of treatment temperature. *Surf. Coat. Technol.* **2005**, *200*, 2474–2480. [[CrossRef](#)]
21. Yang, W.J.; Zhang, M.; Zhao, Y.H.; Shen, M.L.; Lei, H.; Xu, L.; Xiao, J.Q.; Gong, J.; Yu, B.H.; Sun, C. Enhancement of mechanical property and corrosion resistance of 316L stainless steels by low temperature arc plasma nitriding. *Surf. Coat. Technol.* **2016**, *298*, 64–72. [[CrossRef](#)]
22. Alvarez-Fregosa, O.; Chávez-Carvayar, J.A.; Juárez-Islas, J.A.; Camps, E.; García, J.L. FeN and FeN-H thin films prepared by ECR microwave plasma nitriding. *Surf. Coat. Technol.* **1997**, *94–95*, 255–260. [[CrossRef](#)]
23. Krysina, O.V.; Koval, N.N.; Kovalsky, S.S.; Shugurov, V.V.; Lopatin, I.V.; Prokopenko, N.A.; Petrikova, E.A. Low-inertia method of control over nitrogen concentration in the PVD nitride coatings by non-self-sustained arc discharge with thermionic and hollow cathodes. *Vacuum* **2021**, *187*, 110123. [[CrossRef](#)]
24. de la Piedad-Beneitez, A.; Valencia-Alvarado, R.; López-Callejas, R.; Rojas-Olmedo, I.A.; Peña-Eguiluz, R.; Mercado-Cabrera, A.; Barocio, S.R.; Muñoz-Castro, A.E.; Rodríguez-Ménde, B.G. Optimized AISI 304 steel nitriding in inductive RF N₂-H₂ plasmas. *Vacuum* **2011**, *85*, 1149–1151. [[CrossRef](#)]
25. Makówka, M.; Pawlak, W.; Konarski, P.; Wendler, B.; Szymanowski, H. Modification of magnetron sputter deposition of nc-WC/a-C(:H) coatings with an additional RF discharge. *Diam. Relat. Mater.* **2019**, *98*, 107509. [[CrossRef](#)]
26. Grudin, V.A.; Bleykher, G.A.; Krivobokov, V.P.; Semyonov, O.V.; Obroso, A.; Weiß, S.; Sidelev, D.V. Hot target magnetron sputtering enhanced by RF-ICP source: Microstructure and functional properties of CrN_x coatings. *Vacuum* **2022**, *200*, 111020. [[CrossRef](#)]
27. Choe, H.J.; Kwon, S.H.; Lee, J.J. Tribological properties and thermal stability of TiAlCN coatings deposited by ICP-assisted sputtering. *Surf. Coat. Technol.* **2013**, *28*, 282–285. [[CrossRef](#)]
28. Ma, S.; Li, Y.; Xu, K. The composite of nitrided steel of H13 and TiN coatings by plasma duplex treatment and the effect of pre-nitriding. *Coat. Technol.* **2001**, *137*, 116–121. [[CrossRef](#)]
29. Podgornik, B.; Vižintin, J.; Wänstrand, O.; Larsson, M.; Hogmark, S.; Ronkainen, H.; Holmberg, K. Tribological properties of plasma nitrided and hard coated AISI 4140 steel. *Wear* **2001**, *249*, 254–259. [[CrossRef](#)]
30. Baek, W.S.; Kwon, S.C.; Rha, J.J.; Chae, B.G.; Lee, J.Y. Formation mechanism of a black layer between TiN and ion-nitrided steel treated in a duplex process. *Thin Solid Film.* **2003**, *429*, 174–178. [[CrossRef](#)]
31. Tareen, A.K.; Priyanga, G.S.; Behara, S.; Thomas, T.; Yang, M. Mixed ternary transition metal nitrides: A comprehensive review of synthesis, electronic structure, and properties of engineering relevance. *Prog. Solid State Chem.* **2019**, *53*, 1–26. [[CrossRef](#)]
32. Tillmann, W.; Grisales, D.; Stangier, D.; Butzke, T. Tribomechanical behaviour of TiAlN and CrAlN coatings deposited onto AISI H11 with different pre-treatments. *Coatings* **2019**, *9*, 519. [[CrossRef](#)]
33. Domínguez-Meister, S.; El Mrabet, S.; Escobar-Galindo, R.; Mariscal, A.; Jiménez de Haro, M.C.; Justo, A.; Brizuela, M.; Rojas, T.C.; Sánchez-López, J.C. Role of Y in the oxidation resistance of CrAlYN coatings. *Appl. Surf. Sci.* **2015**, *353*, 504–511. [[CrossRef](#)]
34. Berlin, E.V.; Grigoryev, V.J. Plasma Generator. US Patent 9,704,691, 2017.
35. Aghajani, H.; Behrang, S. *Plasma Nitriding of Steels*, 1st ed.; Springer International Publishing: Cham, Switzerland, 2017; pp. 1–67.
36. Kutz, M. *Handbook of Environmental Degradation of Materials*, 2nd ed.; Elsevier Inc.: Amsterdam, The Netherlands, 2013. [[CrossRef](#)]
37. ASTM G102-89; Standard Practice for Calculation of Corrosion Rates and Related Information from Electrochemical Measurements. ASTM International: West Conshohocken, PA, USA, 2004. Available online: <https://www.astm.org/g0102-89r04e01.html> (accessed on 28 October 2022).
38. Cunha, L.; Andritschky, M.; Rebouta, L.; Pischow, K. Corrosion of CrN and TiAlN coatings in chloride-containing atmospheres. *Surf. Coat. Technol.* **1999**, *116*, 1152–1160. [[CrossRef](#)]
39. Shen, H.; Wang, L. Mechanism and properties of plasma nitriding AISI 420 stainless steel at low temperature and anodic (ground) potential. *Surf. Coat. Technol.* **2020**, *403*, 126390. [[CrossRef](#)]
40. Li, Y.; He, Y.; Xiu, J.; Wang, W.; Zhu, Y.; Hu, B. Wear and corrosion properties of AISI 420 martensitic stainless steel treated by active screen plasma nitriding. *Surf. Coat. Technol.* **2017**, *329*, 184–192. [[CrossRef](#)]
41. Nguyen, T.V.; Doan, V.T.; Trinh, T.V.; Vu, H.V. Characteristics of AISI 420 stainless steel modified by combining gas nitriding and CrN coating. *Acta Metall. Slovaca* **2021**, *27*, 146–151. [[CrossRef](#)]
42. Bergelt, T.; Landgraf, P.; Grund, T.; Bräuer, G.; Lampke, T. Modelling of layer development and nitrogen distribution on different microstructures during plasma nitriding. *Surf. Coat. Technol.* **2022**, *447*, 128813. [[CrossRef](#)]
43. Ziegler, J.; Biersack, J.P.; Ziegler, M.D. TRIM (the Transport of Ions in Matter). Available online: www.srim.org (accessed on 28 September 2022).

44. Pizzi, A.; Mittal, K. *Handbook of Adhesive Technology*; CRC Press: Boca Raton, FL, USA, 2017.
45. Xi, Y.T.; Liu, D.X.; Han, D.; Han, Z.F. Improvement of mechanical properties of martensitic stainless steel by plasma nitriding at low temperature. *Acta Metall. Sin. (Engl. Lett.)* **2008**, *21*, 21–29. [[CrossRef](#)]
46. Li, C.X.; Bell, T. Corrosion properties of plasma nitrided AISI 410 martensitic stainless steel in 3.5% NaCl and 1% HCl aqueous solutions. *Corr. Sci.* **2006**, *48*, 2036–2049. [[CrossRef](#)]